Unveiling Nonsecular Collisional Dissipation of Molecular Alignment

Pu Wang,[1] Lixin He,[1,3,*] Yu Deng,[1] Siqi Sun,[1] Pengfei Lan,[1,3,†] and Peixiang Lu[1,2,3,‡]

[1]*Wuhan National Laboratory for Optoelectronics and School of Physics,*
Huazhong University of Science and Technology, Wuhan 430074, China
[2]*Hubei Key Laboratory of Optical Information and Pattern Recognition, Wuhan Institute of Technology, Wuhan 430205, China*
[3]*Hubei Optical Fundamental Research Center, Wuhan 430074, China*

We conducted a joint theoretical and experimental study to investigate the collisional dissipation of molecular alignment. By comparing experimental measurements to the quantum simulations, the nonsecular effect in the collision dissipation of molecular alignment was unveiled from the gas-density-dependent decay rates of the molecular alignment revival signals. Different from the conventional perspective that the nonsecular collisional effect rapidly fades within the initial few picoseconds following laser excitation, our simulations of the time-dependent decoherence process demonstrated that this effect can last for tens of picoseconds in the low-pressure regime. This extended timescale allows for the distinct identification of the nonsecular effect from molecular alignment signals. Our findings present the pioneering evidence that nonsecular molecular collisional dissipation can endure over an extended temporal span, challenging established concepts and strengthening our understanding of molecular dynamics within dissipative environments.

Molecular collisions are ubiquitous in real gas media and play an important role in the molecular dynamics within dissipative environments. The impact of collisions is often manifested through the rapid relaxation of the system, significantly influencing the spectral properties of radiative processes and leading to the redistribution of energy across internal and external degrees of freedom within the system. Unraveling the physical mechanisms underlying collisional dissipation is of great interest and significance, and has stimulated investigations across various scientific fields [1–7].

Over the past few decades, many theoretical and experimental advancements have been made in the exploration of molecular collisional dissipation by leveraging the quantum rotational revivals of molecular alignment in low-pressure gases [8–23]. Studies have demonstrated that molecular collision will lead to the decoherence of the system. Very recently, advances in rotational echo spectroscopy have accessed the exploration of the collisional dissipation in high-density gases within the initial few picoseconds following the pump laser [24–43]. Employing rotational echo spectroscopy, the nonsecular effect in the molecular collisional dissipation process was revealed [31]. This nonsecular effect was observed to systematically slow down collision-induced decoherence processes in the time domain [31]. So far, the nonsecular effect has been exclusively identified in high-pressure gas media using the molecular alignment echo technique [31–35], where its significant role in collisional dynamics has been

widely acknowledged within a few picoseconds after the pump pulse, but dissipating rapidly with the increasing time delay [31–35].

In this Letter, we report the first observation of nonsecular collisional dissipation in the molecular system within the low-pressure regime by employing molecular alignment. Through experimental measurements of molecular alignment signals and a comparison with quantum simulations, the nonsecular effect in the collisional dissipation process of the molecular system in the low-pressure regime was unveiled from the gas-density-dependent decay rates of molecular alignment revivals. Unlike previous findings [31–35], we find that the nonsecular collision effect identified in low-pressure gas media can persist for tens of picoseconds or even longer, and is discernible by measuring the decay of molecular alignment signals. This phenomenon has been experimentally validated in pure N_2, N_2-Ar, N_2-CO_2, and N_2-He mixtures. All the experimental measurements are well supported by the nonsecular quantum simulations. This discovery challenges conventional wisdom, expanding our comprehension of nonsecular effects in molecular collisional dissipation.

In our experiment, the molecular alignment signals were measured by the weak field polarization measurement [44]. Figure 1(a) is the schematic diagram of the experimental setup. The laser source is a commercial Ti:sapphire laser system. It delivers laser pulses at a repetition rate of 1 kHz. The pulse duration and the central wavelength are 35 fs and 800 nm, respectively. The output laser pulse is divided into two beams by a splitter. The pump pulse is linearly
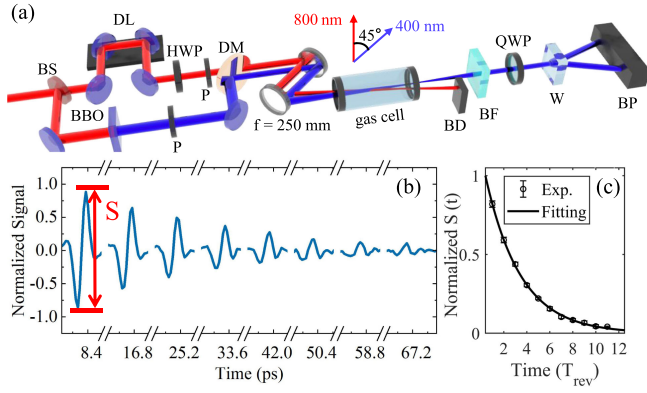
FIG. 1. (a) Schematic diagram of the experimental setup. BD, beam dump; BF, 400-nm bandpass filter; BP, balanced amplified photodetectors; BS, beam splitter; DL, delay line; DM, dichroic mirror; HWP, half-wave plate; P, polarizer; QWP, quarter-wave plate; W, Wollaston prism. (b) Molecular alignment revival signals measured in pure N_2 at room temperature. Here, the gas density is 4.5 amagat. (c) Time-dependent molecular alignment revival intensities (black circles) extracted from (b). Solid line is an exponential fitting of the experimental data.

FIG. 2. (a) Measured (red circles) and calculated [dashed and dotted lines represent the secular (S) and nonsecular (NS) results, respectively] decay rate γ of the alignment revival signals as a function of the gas density in pure N_2. (b) Same as (a) but for γ as a function of the Ar density in the N_2-Ar mixture. (c),(d) Same as (b) but for the N_2-CO_2 and N_2-He mixtures, respectively. In the mixtures, the density of N_2 is fixed at 0.9 amagat. The intercepts of the lines in each panel have been set to zero because we mainly focus on the slopes of these lines.

polarized and the probe pulse is frequency doubled via a β-barium borate (BBO) crystal. The time delay between the pump and probe pulse is controlled by a motorized translation stage. The probe pulse is polarized by a polarizer and set to $\pi/4$ with respect to the pump pulse [see Fig. 1(a)]. These two pulses are focused into a gas cell by a concave mirror ($f = 250$ mm) in a noncollinear geometry. The transmitted probe light is analyzed by a balanced detector which consists of a quarter-wave plate followed by a Wollaston prism and a free-space balanced amplified photodetector as depicted in Fig. 1(a). The signal $I(t)$ measured on the detector is related to the factor of molecular alignment $\langle\cos^2\theta\rangle(t)$, which is given by $I(t) \propto [\langle\cos^2\theta\rangle(t) - 1/3]$.

We first conducted experiments to investigate the molecular collision dynamics with pure N_2 gas. Figure 1(b) depicts the time-dependent molecular alignment revival signals measured with the gas density of 4.5 amagat. We defined the intensity of the molecular alignment revival $S(t)$ as the peak-to-dip amplitude differences of the revival signals. Figure 1(c) show the measured $S(t)$ as a function of pump-probe time delays (black circles). One can clearly see that $S(t)$ decreases monotonically with the time delay. To quantitatively describe the collisional dissipation process, we have performed an exponential fitting $S(t) = A \cdot e^{-\gamma \cdot t/T_{rev}}$ to $S(t)$, as depicted as the solid line in Fig. 1(c). Here $T_{rev} = 8.38$ ps is the rotational period of N_2. The fitting coefficient γ is called the decay rate of the alignment revivals [11].

To study the collisional dissipation process, we have measured the time-dependent molecular alignment revival signals at different gas densities. The corresponding decay rate γ as a function of pure N_2 gas density (red circles) is

depicted in Fig. 2(a). The error bars represent the standard deviations of the fitting results of ten independent measurements. One can see that the decay rate γ increases almost linearly with the density of N_2, which is consistent with previous results [30,32]. We have also performed experiments in N_2-Ar, N_2-CO_2, and N_2-He mixtures. The corresponding decay rate γ as a function of the density of Ar, CO_2, and He in the mixtures is depicted in Figs. 2(b)–2(d), respectively. In the mixtures, the gas density of N_2 is fixed at 0.9 amagat to maintain a consistent contribution of N_2-N_2 interaction to the collisional dissipation process.

For the mixture of N_2 and perturber X with densities d_{N_2} and d_X, the decay rate γ can be written as [11]

$$\gamma(d_{N_2}, d_X) = \gamma^0_{N_2\text{-}N_2} d_{N_2} + \gamma^0_{N_2\text{-}X} d_X, \quad (1)$$

where $\gamma^0_{N_2\text{-}N_2}$ and $\gamma^0_{N_2\text{-}X}$ represent the density-normalized values for N_2-N_2 and N_2-X interactions, respectively. Equation (1) suggests that the decay rate γ in the mixture will increase linearly with the gas density of the perturber. This is well supported by our measurements in Figs. 2(b)–2(d). Note that the slope of the increased decay rate γ just reflects the contribution of N_2-X interaction to the collisional dissipation process [11]. According to Eq. (1), we can get the $\gamma^0_{N_2\text{-}N_2}$ and $\gamma^0_{N_2\text{-}X}$ for N_2-Ar, N_2-CO_2, and N_2-He from Fig. 2, which are 0.0690, 0.0514, 0.0859, and 0.0404 amagat^{-1}, respectively.

To understand the experimental results, we have simulated the time-dependent molecular alignment revival signals with the quantum model [31,35,45,46]. In our simulations, the evolution of the molecular dynamic is described by the density matrix $\rho(t)$ from the Liouville–von Neumann equation:

$$\frac{d\rho(t)}{dt} = -i\hbar[H_0 + H_L(t), \rho(t)] + \left(\frac{d\rho(t)}{dt}\right)_{coll}. \quad (2)$$

Here, H_0 is the molecular free rotation Hamiltonian, and H_L describes the interaction between the molecule and the laser pulse. For the linear molecule and linearly polarized pump laser, $H_L(t) = -\frac{1}{4}E^2(t)\Delta\alpha\cos^2\theta$, where $\Delta\alpha$ is the anisotropy of polarizability of the target molecule and $E(t)$ is the envelope of the laser pulse. The matrix elements of the collisional dissipation can be written as

$$\left(\frac{d\rho_{ij}(t)}{dt}\right)_{coll} = -d\sum_{i',j'}\Lambda_{ij,i'j'}\rho_{i'j'}(t). \quad (3)$$

Here i and j denote the molecular rotational states $|J, M\rangle$ of the system, $\rho_{ij}(t)$ oscillates at angular frequency $\omega_{ij} = (E_i - E_j)/\hbar$, and $\Lambda_{ij,i'j'}$ are the density-normalized relaxation matrix elements constructed as in [31,35]. The parameters for the systems studied here are obtained from Refs. [47–51]. The detailed expression of $\Lambda_{ij,i'j'}$ and the parameters are given in the Supplemental Material [52]. We have performed simulations with both the secular and nonsecular models. In the nonsecular model, all the collisional transfer channels in Eq. (3) are included. In contrast, the secular model disregards the nondiagonal relaxation matrix elements $\Lambda_{ij,i'j'}$ that satisfy $\omega_{ij} \neq \omega_{i'j'}$ [35]. For N_2-X mixtures, $\Lambda_{ij,i'j'} = C_{N_2}\Lambda_{ij,i'j'}^{N_2-N_2} + C_X\Lambda_{ij,i'j'}^{N_2-X}$. C_{N_2} and C_X are the molecular fractions of N_2 and gas X, respectively. $\Lambda_{ij,i'j'}^{N_2-N_2}$ and $\Lambda_{ij,i'j'}^{N_2-X}$ denote the relaxation matrix elements for the N_2-N_2 and N_2-X systems, respectively [49]. The time-dependent alignment factor then is given by

$$\langle\cos^2\theta\rangle(t) = \sum_{J,M}\langle J,M|\rho(t)\cos^2\theta|J,M\rangle$$
$$= \sum_{J,M,J'}\langle J,M|\rho(t)|J',M\rangle\langle J',M|\cos^2\theta|J,M\rangle. \quad (4)$$

We first examined the simulations of pure N_2 with the secular model. The calculated density-dependent decay rate γ is depicted in Fig. 2(a) (black dashed line). Compared to the experimental results, one can see that the decay rate γ simulated by the secular model increases faster with the gas density. To understand this difference, we have also performed simulations with the nonsecular model. The result is shown as the blue dotted line in Fig. 2(a). It can be seen that the nonsecular effect reduces the collisional dissipation and the calculation results agree better with the experimental results. We have also performed the simulations for the gas mixtures. Figures 2(b)–2(d) depict the experimental and calculated results for N_2-Ar, N_2-CO_2, and N_2-He mixtures, respectively. One can see that the results calculated using the secular model also overestimate the slope of the decay rate γ with respect to the gas density
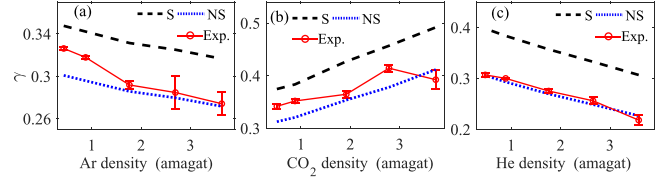
FIG. 3. (a) Measured (red circles) and calculated (dashed and dotted lines represent the secular and nonsecular results, respectively) decay rates γ of the alignment revival signals as a function of the Ar density in the N_2-Ar mixture. Here the total gas density of the gas mixture is fixed at 4.5 amagat. (b),(c) Same as (a) but for the N_2-CO_2 and N_2-He mixtures, respectively.

of the perturber, while the results obtained with the nonsecular model exhibit better agreement with the experimental results. It is worth mentioning that increasing the gas density of the perturber in mixtures amplifies the contribution of N_2-perturber interaction to the collisional dissipation process. The increased decay rates γ as a function of the gas density of the perturber primarily reflect the dissipation induced by the collisions between N_2 and the perturber.

For further evidence, we have also performed experiments and simulations in mixtures with a fixed total gas density (4.5 amagat) while varying the gas densities of N_2 and the perturber. Figures 3(a)–3(c) depict the decay rates γ as a function of the gas density of the perturber in N_2-Ar, N_2-CO_2, and N_2-He mixtures, respectively. One can see that the decay rate γ decreases as the Ar density in N_2-Ar mixtures increases. There is the same trend in N_2-He mixtures. However, in the case of N_2-CO_2 mixtures, the dependence of decay rate γ on the CO_2 density is reversed. The different trend of the gas-density-dependent γ is due to the difference between the contribution of N_2-Ar, N_2-CO_2, and N_2-He interaction to the collisional dissipation process. For the mixture of N_2 and perturber X with a fixed total density d_{total}, the decay rates $\gamma(d_X)$ are given by

$$\gamma(d_X) = \gamma_{N_2-N_2}^0(d_{total} - d_X) + \gamma_{N_2-X}^0 d_X$$
$$= \gamma_{N_2-N_2}^0 d_{total} + (\gamma_{N_2-X}^0 - \gamma_{N_2-N_2}^0)d_X. \quad (5)$$

From Eq. (5), it can be seen that the slope of decay rate $\gamma(d_X)$ is determined by the difference between $\gamma_{N_2-X}^0$ and $\gamma_{N_2-N_2}^0$. According to the results obtained from Fig. 2, we find that $\gamma_{N_2-He}^0$ and $\gamma_{N_2-Ar}^0$ are smaller than $\gamma_{N_2-N_2}^0$, while $\gamma_{N_2-CO_2}^0$ is larger than $\gamma_{N_2-N_2}^0$. Thus a decrease (an increase) trend of the X-density-dependent decay rate γ is observed for N_2-Ar and N_2-He (N_2-CO_2) mixture. With the experimental results in Fig. 3, we can also estimate the $\gamma_{N_2-Ar}^0$, $\gamma_{N_2-CO_2}^0$, and $\gamma_{N_2-He}^0$ from the slopes of γ. The results are 0.0525, 0.0883, and 0.0410 amagat^{-1}, respectively, which are in good agreement with the results obtained from Fig. 2, confirming the consistency between these two independent
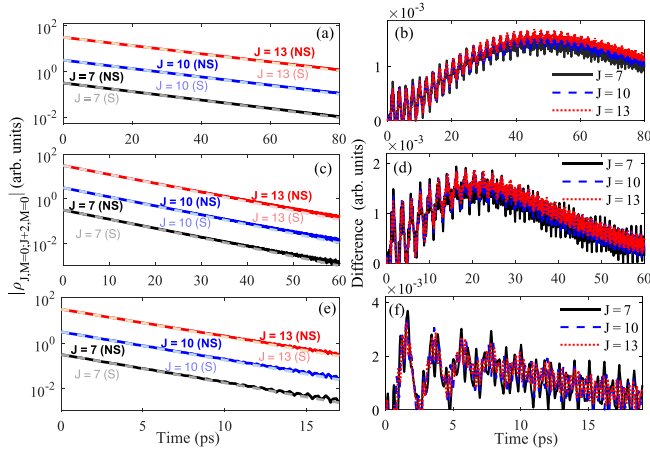
FIG. 4. (a) Modulus of the coherence term $\rho_{J,M=0;J+2,M=0}(t)$ simulated with the nonsecular (solid lines) and secular (dashed lines) models for pure N_2 at 4.5 amagat. For clarity, the results for initial rotational state $|J_0 = J, M_0 = 0\rangle$ with $J = 10$ and $J = 13$ have been multiplied by factors of 10 and 100, respectively. (b) Time-dependent difference of the modulus of the coherence term between the nonsecular and secular models. (c),(d) and (e), (f) Same as (a) and (b) but for 10 and 30 amagat, respectively.

FIG. 5. (a) Molecular alignment revival intensity $S(t)$ simulated by the nonsecular (solid lines) and secular (dashed lines) models for the pure N_2. (b) Difference between the nonsecular and secular results in (a).

measurements. Additionally, we also extracted the corresponding average pressure broadening coefficients by $\Gamma = \gamma_0/(2\pi c T_{\rm rev})$ for these systems. The obtained results are $\Gamma_{N_2\text{-}N_2} = 0.044 \ \text{cm}^{-1}/\text{amagat}$, $\Gamma_{N_2\text{-}Ar} = 0.032 \ \text{cm}^{-1}/\text{amagat}$, and $\Gamma_{N_2\text{-}CO_2} = 0.054 \ \text{cm}^{-1}/\text{amagat}$, which also agree well with the results in previous works [11,48,49].

We have also plotted the simulation results in Fig. 3. As shown, although the secular simulations (S, black dashed lines) can well reproduce the trend of the gas-density-dependent γ, they present much larger deviations in the absolute values of γ. In contrast, the nonsecular results (NS, blue dotted line) agree much better with the experimental results. From the results in Figs. 2 and 3, we concluded that the nonsecular effect in the collisional dissipation process was observed in our molecular alignment experiment on timescales of tens of picoseconds.

For a deep understanding of the nonsecular effect in the collisional dissipation of the molecular alignment, we have further analyzed the time-dependent decoherence process using both nonsecular and secular models. Excited by the linear polarized laser, only the coherence terms $\rho_{J,M;J',M}(t)$ with $J' = J \pm 2$ contribute to the transient alignment revival amplitudes [15]. Therefore, we below focus on these terms. We calculate the modulus of the coherence term $\rho_{J,M=0;J+2,M=0}(t)$ excited from various initial rotational states around the most populated state ($J_0 = 8$) of N_2 at 295 K with different gas densities. Figure 4(a) depicts the modulus of the coherence term $\rho_{J,M=0;J+2,M=0}(t)$ excited from the initial rotational state $|J_0 = J, M_0 = 0\rangle$ at 4.5 amagat. One can see that the time-dependent modulus of the coherence term of nonsecular (solid lines) and secular (dashed lines) models both decrease with time. But the
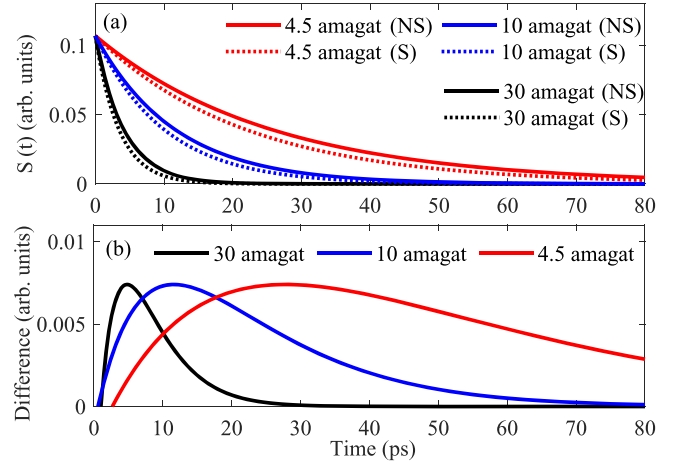
time-dependent modulus of the coherence term in the nonsecular model decreases a little slower than that in the secular model. This can be clearly seen in Fig. 4(b), which plots the time-dependent difference of the modulus of the coherence terms of these two models. A positive difference is observed in Fig. 4(b), indicating the slower decrease induced by the nonsecular effect. Similar results are also observed for higher gas densities, as depicted in Figs. 4(c) and 4(d) for 10 amagat and Figs. 4(e) and 4(f) for 30 amagat. The slower decrease of the coherence term induced by the nonsecular effect consequently slows down the decrease of the alignment signals. In Fig. 5(a), we have simulated the time-dependent molecular alignment signals of pure N_2 with both the nonsecular (solid lines) and secular (dashed lines) models for different gas pressures. It is evident that the nonsecular results decrease slower than the secular results.

In addition, it is crucial to note that for low gas density, as 4.5 amagat in Fig. 5(b), the difference between these two models can keep increasing for a few tens of picoseconds before attenuation. This observation differs from previous findings [31–35]. Such a long-lasting nonsecular effect can thus be accessed by the molecular alignment signals. While for much higher gas density, e.g., 10 and 30 amagat in Fig. 5(b), such difference turns to decrease at earlier time delay. In particular, for 30 amagat, the difference between these two models starts to rapidly decrease at the initial few picoseconds after the pump laser. This is consistent with the previous findings [31–35]. The nonsecular effect at the early stage has been identified by the molecular alignment echo technique [31].

Finally, we should emphasize that our above simulations are performed under the Markov approximation. For the pairs of molecules that interact over long distance, such as $N_2\text{-}CO_2$, the non-Markovian effects could accelerate the

dissipation of the alignment at the early stage of the collision-induced decoherence process [34,35], leading to a much larger decay rate as shown in Fig. 3(b). We can also see that the difference between the nonsecular simulations and experimental measurements is smaller than that between the secular and nonsecular simulations. This result indicates a bigger role of the nonsecularity than the non-Markovianity in our work. Note that developing a quantum model beyond the Markov framework is still a complex problem and has not yet been achieved. It can be anticipated that, by taking the non-Markovian effects into account, the nonsecular simulations of N_2-CO_2 mixture may agree much better with the experimental results.

In summary, the nonsecular effect in the collision dissipation of molecular alignment was first observed. Through a series of proof-of-principle experiments involving pure N_2 gas, N_2-Ar, N_2-CO_2, and N_2-He mixtures, the nonsecular collisional dissipation of molecular alignment is identified. This identification is achieved by comparing the measured gas-density-dependent decay rate of molecular alignment revival signals to the quantum simulations. In contrast to previous investigations utilizing molecular alignment echoes [31–35], our study reveals that the nonsecular collisional effect in the low-pressure regime persists for much longer durations, extending up to tens of picoseconds. The extended temporal persistence of the nonsecular collisional effect uncovered in low-pressure gas media complements existing research, strengthening our comprehension of the intricate dynamics involved in molecular collisional processes.

---

[*]Contact author: helx_hust@hust.edu.cn
[†]Contact author: pengfeilan@hust.edu.cn
[‡]Contact author: lupeixiang@hust.edu.cn

[1] V. May and O. Kühn, *Charge and Energy Transfer Dynamics in Molecular Systems* (John Wiley & Sons, New York, 2023).

[2] J. O. Hirschfelder, C. F. Curtiss, and R. B. Bird, *The Molecular Theory of Gases and Liquids* (John Wiley & Sons, New York, 1964).

[3] I. D. Boyd and T. E. Schwartzentruber, *Nonequilibrium Gas Dynamics and Molecular Simulation* (Cambridge University Press, Cambridge, England, 2017), Vol. 42.

[4] J.-M. Hartmann, C. Boulet, and D. Robert, *Collisional Effects on Molecular Spectra: Laboratory Experiments and Models, Consequences for Applications* (Elsevier, New York, 2021).

[5] Y. Khodorkovsky, U. Steinitz, J.-M. Hartmann, and I. S. Averbukh, Nat. Commun. **6**, 7791 (2015).

[6] U. Steinitz, Y. Khodorkovsky, J.-M. Hartmann, and I. S. Averbukh, Chem. Phys. Chem. **17**, 3795 (2016).

[7] I. Tutunnikov, U. Steinitz, E. Gershnabel, J.-M. Hartmann, A. A. Milner, V. Milner, and I. S. Averbukh, Phys. Rev. Res. **4**, 013212 (2022).

[8] S. Ramakrishna and T. Seideman, Phys. Rev. Lett. **95**, 113001 (2005).

[9] T. Vieillard, F. Chaussard, F. Billard, D. Sugny, O. Faucher, S. Ivanov, J.-M. Hartmann, C. Boulet, and B. Lavorel, Phys. Rev. A **87**, 023409 (2013).

[10] S. Ramakrishna and T. Seideman, J. Chem. Phys. **124**, 034101 (2006).

[11] N. Owschimikow, F. Königsmann, J. Maurer, P. Giese, A. Ott, B. Schmidt, and N. Schwentner, J. Chem. Phys. **133**, 044311 (2010).

[12] R. Damari, D. Rosenberg, and S. Fleischer, Phys. Rev. Lett. **119**, 033002 (2017).

[13] J. Houzet, J. Gateau, E. Hertz, F. Billard, B. Lavorel, J.-M. Hartmann, C. Boulet, and O. Faucher, Phys. Rev. A **86**, 033419 (2012).

[14] G. Karras, E. Hertz, F. Billard, B. Lavorel, J.-M. Hartmann, and O. Faucher, Phys. Rev. A **89**, 063411 (2014).

[15] J.-M. Hartmann and C. Boulet, J. Chem. Phys. **136**, 184302 (2012).

[16] J.-M. Hartmann, C. Boulet, T. Vieillard, F. Chaussard, F. Billard, O. Faucher, and B. Lavorel, J. Chem. Phys. **139**, 024306 (2013).

[17] J.-M. Hartmann, C. Boulet, H. Tran, and M. Nguyen, J. Chem. Phys. **133**, 144313 (2010).

[18] J.-M. Hartmann, C. Boulet, and D. Jacquemart, J. Chem. Phys. **134**, 094316 (2011).

[19] J.-M. Hartmann and C. Boulet, J. Chem. Phys. **134**, 184312 (2011).

[20] J.-M. Hartmann, C. Boulet, H. Zhang, F. Billard, O. Faucher, and B. Lavorel, J. Chem. Phys. **149**, 154301 (2018).

[21] J.-M. Hartmann, C. Boulet, H. Zhang, F. Billard, O. Faucher, and B. Lavorel, J. Chem. Phys. **149**, 214305 (2018).

[22] H. Zhang, F. Billard, O. Faucher, and B. Lavorel, J. Raman Spectrosc. **49**, 1350 (2018).

[23] H. Zhang, F. Billard, X. Yu, O. Faucher, and B. Lavorel, J. Chem. Phys. **148**, 124303 (2018).

[24] G. Karras, E. Hertz, F. Billard, B. Lavorel, J.-M. Hartmann, O. Faucher, E. Gershnabel, Y. Prior, and I. S. Averbukh, Phys. Rev. Lett. **114**, 153601 (2015).

[25] G. Karras, E. Hertz, F. Billard, B. Lavorel, G. Siour, J.-M. Hartmann, O. Faucher, E. Gershnabel, Y. Prior, and I. S. Averbukh, Phys. Rev. A **94**, 033404 (2016).

[26] K. Lin, P. Lu, J. Ma, X. Gong, Q. Song, Q. Ji, W. Zhang, H. Zeng, J. Wu, G. Karras, G. Siour, J.-M. Hartmann, O. Faucher, E. Gershnabel, Y. Prior, and I. S. Averbukh, Phys. Rev. X **6**, 041056 (2016).

[27] K. Lin, J. Ma, X. Gong, Q. Song, Q. Ji, W. Zhang, H. Li, P. Lu, H. Li, H. Zeng, J. Wu, J.-M. Hartmann, O. Faucher, E. Gershnabel, Y. Prior, and I. S. Averbukh, Opt. Express **25**, 24917 (2017).

[28] D. Rosenberg, R. Damari, S. Kallush, and S. Fleischer, J. Phys. Chem. Lett. **8,** 5128 (2017).

[29] D. Rosenberg, R. Damari, and S. Fleischer, Phys. Rev. Lett. **121,** 234101 (2018).

[30] H. Zhang, B. Lavorel, F. Billard, J.-M. Hartmann, E. Hertz, O. Faucher, J. Ma, J. Wu, E. Gershnabel, Y. Prior *et al.*, Phys. Rev. Lett. **122,** 193401 (2019).

[31] J. Ma, H. Zhang, B. Lavorel, F. Billard, E. Hertz, J. Wu, C. Boulet, J.-M. Hartmann, and O. Faucher, Nat. Commun. **10,** 5780 (2019).

[32] J. Ma, H. Zhang, B. Lavorel, F. Billard, J. Wu, C. Boulet, J.-M. Hartmann, and O. Faucher, Phys. Rev. A **101,** 043417 (2020).

[33] J.-M. Hartmann, J. Ma, T. Delahaye, F. Billard, E. Hertz, J. Wu, B. Lavorel, C. Boulet, and O. Faucher, Phys. Rev. Res. **2,** 023247 (2020).

[34] M. Bournazel, J. Ma, F. Billard, E. Hertz, J. Wu, C. Boulet, J.-M. Hartmann, and O. Faucher, Phys. Rev. A **107,** 023115 (2023).

[35] M. Bournazel, J. Ma, F. Billard, E. Hertz, J. Wu, C. Boulet, O. Faucher, and J.-M. Hartmann, J. Chem. Phys. **158,** 174302 (2023).

[36] J. Ma, L. H. Coudert, F. Billard, M. Bournazel, B. Lavorel, J. Wu, G. Maroulis, J.-M. Hartmann, and O. Faucher, Phys. Rev. Res. **3,** 023192 (2021).

[37] B. Wang, L. He, Y. He, Y. Zhang, R. Shao, P. Lan, and P. Lu, Opt. Express **27,** 30172 (2019).

[38] L. Xu, I. Tutunnikov, L. Zhou, K. Lin, J. Qiang, P. Lu, Y. Prior, I. S. Averbukh, and J. Wu, Phys. Rev. A **102,** 043116 (2020).

[39] J. Qiang, I. Tutunnikov, P. Lu, K. Lin, W. Zhang, F. Sun, Y. Silberberg, Y. Prior, I. S. Averbukh, and J. Wu, Nat. Phys. **16,** 328 (2020).

[40] P. Wang, L. He, Y. He, S. Sun, R. Liu, B. Wang, P. Lan, and P. Lu, Opt. Express **29,** 663 (2021).

[41] Z. Lian, Z. Hu, H. Qi, D. Fei, S. Luo, Z. Chen, and C.-C. Shu, Phys. Rev. A **104,** 053105 (2021).

[42] I. Tutunnikov, L. Xu, Y. Prior, and I. S. Averbukh, Phys. Rev. A **106,** L061101 (2022).

[43] P. Wang, L. He, Y. He, J. Hu, S. Sun, P. Lan, and P. Lu, Opt. Lett. **47,** 1033 (2022).

[44] V. Renard, M. Renard, S. Guérin, Y. T. Pashayan, B. Lavorel, O. Faucher, and H.-R. Jauslin, Phys. Rev. Lett. **90,** 153601 (2003).

[45] C. P. Koch, M. Lemeshko, and D. Sugny, Rev. Mod. Phys. **91,** 035005 (2019).

[46] K. Lin, I. Tutunnikov, J. Ma, J. Qiang, L. Zhou, O. Faucher, Y. Prior, I. S. Averbukh, and J. Wu, Adv. Opt. Photonics **2,** 024002 (2020).

[47] L. Bonamy, J. Bonamy, D. Robert, B. Lavorel, R. Saint-Loup, R. Chaux, J. Santos, and H. Berger, J. Chem. Phys. **89,** 5568 (1988).

[48] R. L. Farrow and L. A. Rahn, J. Opt. Soc. Am. B **2,** 903 (1985).

[49] M. Gonze, R. Saint-Loup, J. Santos, B. Lavorel, R. Chaux, G. Millot, H. Berger, L. Bonamy, J. Bonamy, and D. Robert, Chem. Phys. **148,** 417 (1990).

[50] P. Beaud and G. Knopp, Chem. Phys. Lett. **371,** 194 (2003).

[51] P. Beaud, T. Gerber, P. Radi, M. Tulej, and G. Knopp, Chem. Phys. Lett. **373,** 251 (2003).

[52] See Supplemental Material at http://link.aps.org/supplemental/10.1103/PhysRevLett.133.033202 for the details of the construction of the relaxation matrix elements in the simulations.